Lineage segregation in human pre-implantation embryos is specified by YAP1 and TEAD1

Running title: YAP1 and TEAD1 in human embryos

Summary statement: YAP1 and TEAD1 play a role both in the initiation of trophectoderm and the maintenance of primitive endoderm differentiation in human embryos

Marius Regin[1#], Wafaa Essahib[2#], Andrej Demtschenko[1], Delphine Dewandre[1,3], Laurent David[4,5], Claudia Gerri[6,7], Kathy Niakan[6,8], Greta Verheyen[9], Herman Tournaye[9,10], Johan Sterckx[9], Karen Sermon[1&], Hilde Van de Velde[2,9&*]

[1]Research Group Reproduction and Genetics (REGE), Vrije Universiteit Brussel, Laarbeeklaan 103, 1090, Brussels, Belgium

[2]Research Group Reproduction and Immunology (REIM), Vrije Universiteit Brussel, Laarbeeklaan 103, 1090, Brussels, Belgium

[3]Current address: Beacon CARE Fertility, Beacon Consultants Concourse, Sandyford, Dublin, Ireland

[4]Nantes Université, CHU Nantes, Inserm, CR2TI, UMR 1064, F-44000 Nantes, France

[5]Nantes Université, CHU Nantes, Inserm, CNRS, BioCore, F-44000 Nantes, France

[6]Human Embryo and Stem Cell Laboratory, The Francis Crick Institute, 1 Midland Road, London NW1 1AT, UK

[7]Present address: Max Planck Institute of Molecular Cell Biology and Genetics, Pfotenhauerstrasse 108, 01307, Dresden, Germany

[8]Centre for Trophoblast Research, Department of Physiology, Development and Neuroscience, Cambridge, UK

[9]Brussels IVF, Universitair Ziekenhuis Brussel, Laarbeeklaan 101, 1090, Brussels, Belgium

[10]Department of Obstetrics, Gynaecology, Perinatology and Reproduction, Institute of Professional Education, Sechenov First Moscow State Medical University of the Ministry of Health of the Russian Federation, Trubetskaya str., 8, b. 2, 119992, Moscow, Russia

[#]And [&] contributed equally to the work

*Corresponding author: hilde.vandevelde@uzbrussel.be

Abstract

We know that polarity and YAP1 play a key role in trophectoderm initiation in compacted human embryos, however we know little about the TEAD family of transcription factors that become activated by YAP1 and especially if they play a role during epiblast and primitive endoderm formation.

Here we show that compaction occurs heterogeneously between the 8- and 16-cell stages. While 8-cell stage blastomeres are not yet polarized, polarized outer cells and non-polarized inner cells arise in compacted 16-cell stage embryos, however, they do not arise by symmetric and asymmetric divisions. While trophectoderm specifiers TEAD1, YAP1 and GATA3 mostly co-localise in the nuclei of polarized outer/trophectoderm cells, they are also found in some cells of compacting embryos before polarity is established indicating that differentiation into trophectoderm cells can be initiated independently of polarity. In the inner cell mass, TEAD1 and YAP1 also distinguish GATA4 positive cells in a salt-and-pepper distribution and in the sorted primitive endoderm cells. We suggest that TEAD1/YAP1 signalling plays a role both in the initiation of trophectoderm and the maintenance of primitive endoderm differentiation.

54 **Introduction**

55 Although extensively studied in the mouse model, the molecular events driving
56 lineage segregation to either trophectoderm (TE), epiblast (EPI) or primitive endoderm
57 (PrE) cells in human embryos remain largely unknown. In the mouse, the Hippo
58 signalling pathway plays a crucial role in both TE and EPI differentiation, with the TEA-
59 domain transcription factor family (TEAD1-4) and co-activator Yes-associated-protein
60 1 (YAP1) as key components (Nishioka *et al.*, 2008, 2009; Ralston *et al.*, 2010; Hirate
61 and Sasaki, 2014; Hashimoto and Sasaki, 2019). Differences in cell polarity drive the
62 first lineage differentiation event in the mouse. Mouse embryos compact at the 8-cell
63 stage with all blastomeres being polarized (Levy *et al.*, 1986). Polarity is marked by the
64 presence of an apical cap composed of the PAR complex proteins (PAR3, PAR6 and
65 atypical Protein Kinase C (aPKC)) and p-ERM, which is a component of the microvilli
66 linking F-actin to the apical membrane (Plusa *et al.*, 2005; Alarcon, 2010; Zhu *et al.*,
67 2017). During the 8- to 16-cell stage divisions, a symmetric division through the
68 meridian yields two daughter cells with a polar cap that are located in an outer position.
69 After an asymmetric division through the equator, cells that inherit the polar cap remain
70 in an outer position whereas non-polarized cells are relocated towards an inner
71 position (Johnson and Ziomek, 1981; Anani *et al.*, 2014; Lorthongpanich and
72 Issaragrisil, 2015). This is crucial for establishing an inner/non-polarized and
73 outer/polarized cellular axis in the mouse embryo. Non-polarized inner cells exclude
74 YAP1 from the nuclei through phosphorylation of serine127 by the large tumour
75 suppressor protein kinase (LATS1/2). Consequently, *Cdx2* expression is
76 downregulated, whereas SOX2 protein levels increase maintaining pluripotent inner
77 cells and rendering them precursors of the ICM (Wicklow et al., 2014). In contrast, in
78 polarized outer cells LATS1/2 activity is restricted by the presence of the polar region
79 and TEAD4/YAP1 nuclear activity leads to the upregulation of *Cdx2* and *Gata3*
80 expression (Nishioka *et al.*, 2008, 2009; Ralston *et al.*, 2010; Hirate and Sasaki, 2014).
81 This first lineage segregation event is also regulated by other mechanisms such as
82 cortical tension (Maître *et al.*, 2015; Maître, 2017; Zhu *et al.*, 2017).

83 In the mouse, the second lineage segregation event is regulated by the
84 FGF4/FGFR2 signalling pathway (Chazaud *et al.*, 2006; Yamanaka, Lanner and
85 Rossant, 2010). In ICM cells, the NANOG positive precursor EPI cells secrete FGF4
86 for which the GATA6 positive precursor PrE cells have FGF2R receptors. The EPI and
87 PrE cells first display a salt-and-pepper pattern whereafter the cells are sorted into an

88 inner population of EPI cells are covered by a monolayer of PrE cells facing the cavity.
89 Recently TEAD1/YAP1 signalling has also been found to play a role in the
90 establishment of the EPI cells (Hashimoto and Sasaki, 2019), but it is not known how
91 the two signalling pathways act together.

92 Recent single cell transcriptomic analysis of human embryos gave also insight
93 into transcription factors that are associated with each lineage differentiation events
94 (Yan *et al.*, 2013; Blakeley *et al.*, 2015; Petropoulos, 2016; Stirparo *et al.*, 2018;
95 Meistermann *et al.*, 2021; Radley, Smith and Dunn, 2022). We and others
96 demonstrated by careful embryo staging using morphokinetic analysis that human
97 embryos initiate compaction at variable times between the 8- and the 16-cell stage
98 (Gerri *et al.*, 2020). The first lineage differentiation in compacted human embryos is
99 orchestrated by polarity and involves YAP1 and GATA3 signalling (Gerri *et al.*, 2020)
100 and phospholipase C signalling (Zhu *et al.*, 2021). Few data are available on the
101 second lineage differentiation in human blastocysts, but it appears independent of FGF
102 signalling (Kuijk *et al.*, 2012; Roode *et al.*, 2012). Based on single-cell transcriptomics
103 data, competing hypotheses on the second lineage differentiation in human blastocysts
104 have been proposed. According to the one step model, EPI and PrE lineages arise
105 simultaneously with TE cells 5 days post fertilisation (dpf) (Petropoulos, 2016) whereas
106 according to the two step model the first and the second lineage differentiation events
107 appear consecutively (Meistermann *et al.*, 2021) as in mice (Chazaud and Yamanaka,
108 2016). It is also unclear whether ICM cells segregate into EPI and PrE cells (Radley *et*
109 *al.*, 2022) as in mice (Chazaud and Yamanaka, 2016) or whether PrE cells differentiate
110 from the EPI cells on 6 dpf (Meistermann *et al.*, 2021). This lack of clarity may have
111 been caused by the heterogeneous development of outbred human embryos *in vitro,*
112 different laboratory culture conditions and the lack of systematic coupling of
113 morphology with the underlying analysis. Moreover, limited data are available on the
114 transcription factors and signalling pathways at the protein level and very few functional
115 studies have been performed.

116 Our current aim was to provide a comprehensive spatial and temporal map of
117 the processes of compaction, polarisation, position and blastulation, and the first and
118 second lineage differentiation events in human pre-implantation embryos. Through the
119 investigation of the main proteins in well-defined human pre-implantation stages we
120 demonstrate a human specific chain of events during compaction and polarisation in
121 outer and inner cells. We also reveal that both TE and PrE lineage segregation in

122 human pre-implantation embryos are specified by transcription factor TEAD1 and co-
123 activator YAP1.
124

125 **Results**

126 **Inner and outer cells are established in the compacted human embryo**
127 In order to establish the number of cells at each embryonic developmental stage as
128 described in the clinical grading system, we first analysed the appearance and the
129 number of inner and outer cells in relation to the total number of cells by confocal
130 microscopy (Fig. 1). Cell counts were determined by analysing confocal Z-stack scans
131 for nuclear Hoechst and membrane F-actin staining (Fig. 1A).
132 We observed no inner cells, defined as cells completely separated from the perivitelline
133 space, during the compaction process (Fig. 1D, Fig. 2A). At the onset of compaction
134 (C0), the embryos contained 10.9±2.5 cells and compacting C1 embryos contained
135 13.6±2.1 cells (Fig. 1B). The first inner cells were observed in the fully compacted C2
136 embryos, which on average contained a total number of 18.9±6.1 cells (Fig. 1B), and
137 showed a range of inner cells between 0 (5/30 embryos) and 6 (Fig. 1D), with a mean
138 of 2.3±0.7, while 16.8±4.7 cells were outer cells (Fig. 1E).
139 When small cavities appeared, the outer cells changed morphologically into sickle-
140 shaped cells (Fig. 1A, B0, white star). The total number of cells increased from an
141 average of 28.1±7.8 cells at the onset of blastulation (B0) to 54.8±13.7 in full
142 blastocysts (B1/2) and 81.4±14.8 (B3) upon expansion at 5 dpf and to 155.4±39.5 in
143 fully expanded blastocysts (B4/5/6) at 6 dpf (Fig. 1C). By comparing the cell counts for
144 inner/ICM and outer/TE cells throughout development, we observed that while the
145 number of inner/ICM cells followed a linear increase, the number of outer/TE cells
146 increased exponentially (Fig. 1D-E). We conclude that compaction occurs
147 heterogeneously, i.e. without apparent established course of events, between the 8-
148 and 16-cell stages and inner cells first appear in compacted human embryos.
149

150 **Polarity marker p-ERM is apically localised in outer cells of compacted human**
151 **embryos and precedes F-actin**
152 We aimed to identify differences in apical polarity between inner and outer cells
153 throughout human pre-implantation development by co-staining for F-actin and p-ERM.
154 F-actin has already been used as an apical marker in human embryos by Zhu et al.

155 (Zhu *et al.*, 2021); p-ERM has not yet been investigated in human embryos but is well-
156 described in the mouse model (Anani *et al.*, 2014; Zhu *et al.*, 2020).

157 First, we determined the spatial and temporal localisation of F-actin during
158 human pre-implantation development (Fig. 1A, Fig. 2A-B). While in oocytes and
159 cleavage-stage embryos F-actin was mainly diffuse in the cytoplasm, it became
160 concentrated at the cortex of all the cells at the start of compaction (C0) to remain there
161 during the compaction process (C1). F-actin started to appear concentrated in the
162 apical region of outer cells when compaction was completed (C2) and it gradually
163 increased at the start of cavitation in B0 blastocysts; in C2 and B0 stages F-actin also
164 appeared as a ring around the nucleus. In B1 blastocysts F-actin was apically polarized
165 in all the outer cells. From the B1 blastocyst stage onwards it became gradually
166 concentrated in the intercellular junctions between the sickle-shaped outer cells.
167 Finally, F-actin was highly concentrated in the junctions of the TE cells (B2-B6) but
168 remained perinuclear and at the cortex in the ICM cells in full B2 and expanding B3
169 blastocysts (Figure 2A) and in inner cells of expanded B4 and hatching/hatched B5/B6
170 blastocysts (Figure 1A). We conclude that F-actin is localised apically in all the
171 outer/TE cells from the early B1 blastocyst stage onwards.

172 Next, we analysed the pattern of p-ERM during pre-implantation development
173 (Fig 2A-B). Diffuse presence of p-ERM without polarity was observed in oocytes and
174 blastomeres of cleavage-stage embryos. P-ERM gradually became localised at the
175 cell-contact-free surface during compaction in C0 and C1 embryos without reaching
176 apical polarity. Full apical polarity of p-ERM was observed in all outer cells of all
177 compacted C2 embryos, while it was absent at sites of cellular contact. P-ERM
178 remained apical in early blastocysts (B0 and B1), then shifted from the apical cap to
179 intercellular regions during blastocyst expansion (B2-B3). We conclude that p-ERM is
180 localized in the apical cap of all outer cells in compacted C2 embryos and blastocysts.

181 Since the immunofluorescence analysis suggested that p-ERM polarity
182 precedes F-actin polarity, we analysed the co-localisation of p-ERM and F-actin to
183 define the precise order (Fig. 2A and Fig2C). At the compacted C2 stage all outer cells
184 had an apical p-ERM cap, but only 42.2% of these cells had polarized F-actin, while
185 this number rose to 65.4% of outer cells in the early B0 blastocysts which that showed
186 apical co-localisation of p-ERM expression is and F-actin, suggesting that p-ERM
187 polarizes before F-actin ($p<0.00001$, Fisher-exact-test). From the B1 blastocyst stage
188 onwards, p-ERM and F-actin co-localized in the apical cap of all outer cells. We

189 observed a shift of p-ERM distribution from the apical surface of the blastomeres to
190 sites of intercellular contact coinciding with F-actin re-allocation during blastocyst
191 expansion (B2/B3) (Fig 2A-B). We conclude that p-ERM polarisation is completed by
192 the compacted stage in human embryos and precedes F-actin apical polarity.
193
194 **Nuclear YAP1 precedes polarity and mainly specifies polarized outer/TE cells**
195 Because of their important role in cellular polarity and lineage segregation in the
196 mouse, we co-stained for p-ERM and YAP1 (Fig. 3A). While few cells (19.5%) were
197 positive for nuclear YAP1 at the start of compaction (C0), their number markedly
198 increased (56.1%) at the compacting embryo stage (C1) in the presence of non-
199 polarized p-ERM (Fig. 3B). At the compacted embryo stage (C2), all outer cells were
200 polarized and most of these cells (84.6%) displayed high levels of nuclear YAP1; all
201 inner cells were non-polarized and in 25% of these cells nuclear localization of YAP1
202 was found (Fig. 3C, C2 panel). In general, throughout the blastocyst stages B0-B3 on
203 5 dpf, all embryos showed polarized outer/TE cells positive for YAP1 and non-polarized
204 inner/ICM cells negative for YAP1 (Fig. 3D). The outer cells of B0 embryos contained
205 the largest number of cells that were mostly YAP1 positive and polarized (99%) with
206 the exception of one non-polarized cell. The majority of inner cells lacked YAP1 and
207 polarity (84%) but in rare cases they were YAP1 positive and non-polarized (4%) or
208 polarized (12%) (Fig. 3C, Fig. S1A, first row). At the B1-B3 stage, we found that 97.1%
209 of the outer/TE cells were polarized and YAP1 positive in B1, 94.8% in B2 and 95% in
210 B3. Most non-polarized inner/ICM cells lacked YAP1: 100% at B1, 97.6% at B2 (with
211 the exception of one cell that was polarized and YAP1 positive) and 100% at B3.
212 Throughout the blastocyst stages, we also found a small population of polarized TE
213 cells negative for YAP1 (3.4%) (Fig. S1A, second row). We conclude that nuclear YAP1
214 may precede the establishment of the apical polar cap and becomes mainly restricted
215 to polarized outer/TE cells from the compacted embryo stage onwards.
216
217

218 **GATA3 follows YAP1 expression in outer cells and co-localize in trophectoderm**
219 The establishment of a high-resolution time frame of the appearance of cell polarisation
220 and nuclear YAP1 localisation throughout human pre-implantation development
221 allowed us to match the appearance of YAP1 with GATA3, the first transcription factor
222 associated with trophectoderm specification in the human embryo (Gerri et al., 2020).
223 Confirming our findings shown in Fig 3A-B, the presence of YAP1 positive nuclei
224 was observed at the early compaction stages in 34.1% of cells at C0 and 44.2% at C1
225 in all embryos (Fig 4A-B). Nuclear GATA3 was first detected at low levels in two out of
226 four compacting C1 embryos in a few cells (11.6%) and always co-localised with
227 nuclear YAP1 (Fig. 4A-C). Throughout compaction, we never observed YAP1-
228 /GATA3+ nuclei. Once distinguishable inner cells were formed at the compacted C2
229 stage, most of the embryos (n=5/8) showed differential levels of YAP1 and GATA3
230 between the inner and outer cells. GATA3 was completely absent from inner cells and
231 most inner cells lacked both proteins (75.0%) while 25% were positive for YAP1 only
232 (Fig. 4C; Fig. S1A, C2), as found in previous immunofluorescence analysis (Fig. 3C).
233 At the C2 stage, 26.1% of the outer cells were still negative for both YAP1 and GATA3
234 (Fig. S1B, C2), 73.9% of the cells showed nuclear YAP1 only and in 21.8% of the cells
235 YAP1 and GATA3 co-localized (Fig. 4C). The differential pattern between inner and
236 outer cells became more pronounced during the transition to the blastocyst stages (B0-
237 B3) (Fig. 4D). Most of the B0 cells were outer cells (83.4%), of which half were YAP1
238 positive only, 35.9% were YAP1/GATA3 positive (Fig. 4D) and 14.1% lacked either
239 proteins (Fig. S1B). During the following blastocyst stages the percentages of TE cells
240 containing both YAP1 and GATA3 increased: 95.2% in B1, 94.6% in B2 and 97.3 % in
241 B3. Conversely, the percentage of outer/TE cells that contained YAP1 only decreased:
242 0.8 % in B1, 4.1% in B2 and 0.5% in B3. Furthermore, outer/TE cells that lacked both
243 proteins decreased during blastocyst expansion: 4% in B1, 1.4% in B2 and 2.2% in B3.
244 While the TE cells displayed YAP1/GATA3 in almost all nuclei by the B3 stage, the
245 inner/ICM cells remained negative for both proteins with few exceptions: 87.1% in B0,
246 93.2% in B1, 89.2% in B2 and 96.2% in B3. Notably, some rare inner/ICM cells were
247 either GATA3 and/or YAP1 positive: B0 (12.9%), B1 (6.8%), B2 (10.7%) and B3 (3.8%)
248 (Fig. 4D; Fig. S1B, B1 panel). The percentage of YAP1 positive cells as well as the
249 nuclear intensity for YAP1 increased between the C0 and C1 stages, and YAP1
250 appearance preceded GATA3 that became more prominent in C1 (Fig 4B-E). Between
251 C2 and B0, YAP1 and GATA3 became more restricted to the outer cells, with a clear

252 decline in the inner cells. These results confirm reported single cell transcriptomics
253 data (Meistermann *et al.*, 2021) (Fig. S2A-B). YAP1 and GATA3 proteins were absent
254 in oocytes (Fig. S3A). We conclude that YAP1 and GATA3 can be found in the nuclei
255 of compacting embryos before polarity is fully established, and that the presence of
256 nuclear YAP1 precedes the appearance of GATA3.
257
258 **Outer and inner cells do not arise through symmetric and asymmetric divisions**
259 **in the compacted human embryo**
260 We demonstrated that in human 8-cell stage embryos the blastomeres are non-
261 polarized (Fig 3A) and compaction and polarization occur heterogeneously between
262 the 8- and 16-cell stages (Fig 1-2). Moreover, nuclear YAP1 is mainly present in outer
263 cells but it is also detected in 25% of the inner cells of C2 compacted embryos (Fig 3C
264 and Fig 4C). Therefore, it is unlikely that outer and inner cells are generated through
265 symmetric and asymmetric divisions as in the mouse. These divisions have been
266 thoroughly studied in isolated 8-cell stage mouse blastomeres (Dietrich and Hiiragi,
267 2007; Lorthongpanich *et al.*, 2012; Anani *et al.*, 2014).
268 To investigate the divisions in human embryos, we split 8-cell stage (n=4), 9-cell stage
269 (n=2) and 10-cell stage (n=1) embryos into single blastomeres by micromanipulation
270 and analysed the dividing blastomeres by time lapse. Sixty isolated blastomeres
271 devoid of any cell-cell contact were cultured and the ensuing 2/16 couplets
272 representing two cells from a 16-cell stage embryo were carefully studied as they
273 developed into mini-blastocysts (Fig. 5A, Supplementary videos 1-2). After
274 manipulation, 5/60 cells lysed (8.4%) and 4/60 cells failed to form couplets (6.7%).
275 After excluding three cells that were already 2/16 couplets at the start of culturing, we
276 analysed a total of 48 blastomeres (80%). Two major patterns could be observed in
277 the isolated dividing cells. In pattern I (31/48 cells or 64.6%), after the first division
278 (15h), the two cells of the 2/16 couplets adhered firmly to each other and one cell
279 engulfed the other cell around 25h (Fig. 5A, pattern I, Supplementary Video 3). During
280 the following division, the mini-embryos started to cavitate, the engulfing cell developed
281 into sickle-shaped TE cells whereas the engulfed cell developed into round ICM cells
282 (41.8h). In pattern II (17/48 cells or 35.4%), the 2/16 couplets (at around 17.5h)
283 increased cell contact but no engulfment was observed, the mini-embryos divided into
284 4/32 quadruplets (34.7h), subsequently compacted (38.1h) and blastulated (46.3h)
285 without ICM formation (Fig. 5A, pattern II, Supplementary Video 4). These

286 observations suggested that 2/16 couplets undergoing pattern I formed both TE and
287 ICM cells while 2/16 couplets following pattern II developed into TE cells only. It is
288 tempting to propose that pattern I and II represent an asymmetric and symmetric
289 division, respectively.

290 To investigate this, we repeated the experiment followed by immunostaining. In
291 2/16 couplets following pattern I, the engulfed inner cells were non-polarized, as
292 evidenced by an absent p-ERM cap, and lacked nuclear YAP1 in contrast to the
293 polarized engulfing outer, YAP1 positive, cells (Fig. 5B, pattern I). In line with our
294 observations in blastocysts, we identified an inner cell in a mini-blastocyst that was
295 negative for both YAP1 and GATA3 on 5 dpf (Fig. 5C, pattern I, top row), while we also
296 observed NANOG positive ICM cells in mini-blastocysts on 6 dpf (Fig. 5C, pattern I,
297 bottom row). In 2/16 couplets following pattern II, the non-polarized and polarized cell
298 were both positive for YAP1 while in the 4/32 quadruplets all cells were polarized with
299 a visible p-ERM cap and nuclear YAP1 (Fig. 5B, pattern II). At 6 dpf mini-blastocysts
300 that morphologically lacked ICM cells also lacked NANOG positive cells (Fig. 5C,
301 pattern II). Based on these stainings we conclude that pattern I represents an
302 asymmetric division and pattern II represents a symmetric division.

303 Only one embryo (n°4) contained blastomeres that displayed both patterns (Fig. 5D),
304 which confirms our conclusion. We observed a clear segregation between embryos
305 whose single blastomeres all followed pattern I (4/7) and embryos (2/7) where all single
306 blastomeres followed pattern II. To compare the two patterns, we assessed whether
307 there was a difference in the timing of start of the compaction and blastulation, which
308 are established quality markers in IVF clinics (Skiadas, Jackson and Racowsky, 2006;
309 Iwata *et al.*, 2014; Motato *et al.*, 2016; Rienzi *et al.*, 2019; Harada *et al.*, 2020). We
310 determined t=0 as the timepoint when the first 1/8 blastomere from an individual
311 embryo was dividing into a 2/16 couplet. The mini-blastocysts that underwent pattern
312 I compacted earlier ($p<0.0001$, mean (pattern I = 8.6h vs pattern II = 20.8h) (Fig. 5E)
313 and cavitated earlier ($p<0.0001$, mean (pattern I =16.5h vs pattern II =28.2h) (Fig. 5F)
314 than the ones that underwent pattern II. We observed no significant differences in the
315 duration of compaction to cavitation between both patterns (mean pattern I = 7.7h vs
316 pattern II = 7.4h) (Fig. 5G). Since we demonstrated that cavitation normally starts
317 around the 32-cell stage (Fig. 1C), we suggest that pattern II development is delayed
318 and abnormal and pattern I development is normal. Moreover, pattern I results in the
319 formation of both ICM and TE. Because the 8-cell stage blastomeres all divide in the

320 same way, we conclude that outer cells and inner cells are not generated through
321 symmetric and asymmetric divisions.
322
323 **TEAD1/YAP1 co-localisation is restricted to trophectoderm and primitive**
324 **endoderm cells**
325 YAP1 is co-activator of the TEAD1-4 family of transcription factors. Recently we
326 showed that in the human embryo TEAD4 proteins are present in all nuclei at the fully
327 compacted embryo stage (Gerri *et al.*, 2020). To better understand how TEAD4 is
328 involved in lineage segregation throughout human pre-implantation development, we
329 performed immunofluorescent analysis of TEAD4, p-ERM and GATA3. Low levels of
330 TEAD4 proteins first appeared in all nuclei during compaction (C1) and they were
331 ubiquitously present in the nuclei of all the cells throughout pre-implantation
332 development from the compacted stage onwards (C2-B6) (Fig. 6A-B). This confirmed
333 the single-cell RNAseq data of (Meistermann *et al.*, 2021)(Fig S2A-B).
334 Transcriptomics data suggest that other members of the TEAD family may play
335 a role during human pre-implantation development as well, specifically TEAD1 stood
336 out as a specific regulator of TE and potentially PrE (Yan *et al.*, 2013; Stirparo *et al.*,
337 2018; Meistermann *et al.*, 2021). We also selected TEAD1 for further study because
338 already been found to play a role in the second lineage segregation in the mouse
339 (Hashimoto and Sasaki, 2019). TEAD1 displayed a spatial and temporal pattern that
340 was distinct from TEAD4. TEAD1 was found in 65.5% of the nuclei of the cells already
341 at the start of compaction (C0) and in all the cells during compaction (C1) (Fig. 6C, Fig.
342 S4A). From the compacted C2 stage onwards TEAD1 proteins were abundantly
343 present in the outer and TE cells up to 6 dpf (B0-B4) (Fig. 6C, Fig. S4B, S4C). At the
344 compacted C2 stage, however, only 11.8% of the inner cells were positive for TEAD1.
345 This TEAD1 expression pattern coincided with YAP1/GATA3 co-localisation in the
346 outer cells (Figure 4A). Most outer/TE cells throughout the B0-B3 blastocyst stages
347 were positive for TEAD1; 100% in B0-B2 and 98.1% in B3. Therefore, we suggest that
348 TEAD1/YAP1 interaction plays a role in the initiation of TE formation. However, TEAD1
349 proteins were also detected in most nuclei of the inner/ICM cells of the blastocysts on
350 5 dpf from cavitation onwards, 83.3% in B0, 91.3% in B1, 92.9% in B2 and 83.6% in
351 B3 (Fig 6C, 6E), but at visibly lower levels as compared to TE cells (Fig. 6C).
352 By fine-mapping TEAD1, we noticed increased signals of nuclear localisation of this
353 transcription factor in B4 and later blastocysts in cells that could correspond to PrE. In

354 B4 blastocysts, we found TEAD1 positive and negative cells in a heterogeneous
355 pattern (Fig. S4B) and in the cells facing the cavity (Fig. S4C). Strikingly, the increase
356 in the levels of TEAD1 proteins in the ICM cells coincided with the appearance of
357 nuclear YAP1 in these cells (Fig. S4B). In YAP1 positive cells the epiblast marker
358 NANOG was absent (Fig. S4C) but the primitive endoderm marker SOX17 was
359 detected (Fig. S4D). Because this pattern is reminiscent of the second lineage
360 segregation, we hypothesised that TEAD1/YAP1 expressing cells in the ICM of
361 expanding blastocysts could be (precursor) PrE-cells.
362 To test this hypothesis, we first assessed the presence of NANOG during the
363 compaction (C0-C2) and early blastulation stages (B0-B1). After extensive antibody
364 validation (Fig. S4E-G), NANOG was found to be absent at all compaction stages (Fig.
365 S4E). At the B0-B1 blastocyst stages we found NANOG positive and negative nuclei
366 in the ICM cells as well as in the TE cells (Fig. S4F). Furthermore, from the B3
367 blastocyst stage on, we stained for EPI (NANOG) and PrE (SOX17 and GATA4)
368 markers. In the ICM of B3 blastocysts we found one main population of cells with
369 NANOG+/SOX17-/GATA4- nuclei (89.1%) (Fig. 7A, 7B). The B3 ICM consisted of four
370 additional minor subpopulations: NANOG+/SOX17+/GATA4- cells (5.4%), NANOG-
371 /SOX17-/GATA4- cells (3.9%) and cells in which exceptionally NANOG, SOX17 and
372 GATA4 (0.8%) and GATA4 and SOX17 only co-localized (0.8%) (Fig. 7B, Fig. S5A-D).
373 In seven out of nine B3 blastocysts, nuclear NANOG was found in all the ICM cells
374 (Fig. 7A). Based on all our observations on the second lineage segregation we
375 assessed the average number of cells in the EPI (12.1±6.5 cells) and PrE-lineage
376 (8.4±3.44 cells) at 6dpf (Fig. 7C). At 6 dpf the ICM consisted of two populations only:
377 NANOG+ cells (EPI) and SOX17+/GATA4+ cells (PrE) either in salt-and-pepper (Fig.
378 7D) or in segregated populations (Fig. 7E). We also detected GATA3 positive cells co-
379 localizing with SOX17 (27%) (Fig. S5E), which were also found in reported single-cell
380 RNAseq data (Meistermann *et al.*, 2021) (Fig S2A-B).
381 To investigate the (precursor) PrE-population further, we co-stained ~~5 dpf and 6 dpf~~
382 blastocysts for TEAD1, YAP1 and GATA4 (Fig. 7F-I). We identified two main cell
383 populations in the ICM of B4-6 blastocysts (Fig. 7F, G): cells negative for all markers
384 that we considered the EPI lineage (46.5%) and cells positive for all three markers that
385 we considered the PrE-lineage (28.1%). We also observed three subpopulations in the
386 ICM cells that consisted of TEAD1+/YAP1+/GATA4- cells (14%), TEAD1+/YAP1-
387 /GATA4+ cells (7%) and TEAD1+/YAP-/GATA4- cells (4.4%). From this pattern it

388 became clear that in the majority of the GATA4 positive PrE-cells co-localisation of
389 TEAD1/YAP1 was found. However, GATA4 was also found in the absence of
390 TEAD1/YAP1 co-localisation (7%), suggesting that TEAD1/YAP1 interaction may play
391 a role in the maintenance of the PrE-lineage rather than in the initiation of the second
392 lineage differentiation. Finally, to further elucidate whether the TEAD1/YAP1
393 interaction initiates or maintains the PrE-lineage, we analysed embryos from the C0 to
394 the B3 stages for TEAD1, YAP1 and GATA4 (Fig. 7H, 7I, S5F). GATA4 was first
395 detected in ICM cells of B2 (2.4%) and B3 (7.1%) blastocysts when TEAD1 signals
396 were visibly weak and YAP1 was undetectable (Fig. 7H, 7I). Cells positive for all three
397 markers only arise later at B4-6 stage (Fig. 7F, G). Therefore, we conclude that
398 TEAD1/YAP1 interaction plays a role in the maintenance rather than in the initiation of
399 PrE-formation.
400
401 **Discussion**
402 We show that in human pre-implantation embryos, which compact and polarise
403 heterogeneously between the 8- to 16-cell stages, the formation of a p-ERM apical cap
404 precedes the concentration of F-actin at the apical region. YAP1 and GATA3 co-
405 localize in the polar outer cells, supporting the role of polarity in TE initiation. However,
406 they also co-localize in the nuclei of some blastomeres before the cells are polarized,
407 indicating that the first lineage differentiation event can be initiated independently of
408 polarity. We also show that outer and inner cells, which appear in the compacted
409 embryo, do not arise by symmetric and asymmetric divisions. Finally, based on spatial
410 and temporal mapping we suggest for the first time a role for TEAD1/YAP1 interaction
411 in both the initiation of TE and maintenance of PrE differentiation in human pre-
412 implantation embryos.
413 Compaction and polarisation coincide in human embryos, as in the mouse (Levy
414 *et al.*, 1986), but by using morphokinetics it was demonstrated that the human
415 compaction process is heterogeneous (Gerri *et al.*, 2020). We confirmed this by use of
416 F-actin staining and we also showed that, as reported in the mouse (Dietrich and
417 Hiiragi, 2007), inner and outer cells are established in the compacted 16-cell stage
418 embryo. We demonstrated polarity by the presence of p-ERM proteins at the apical
419 cortex of the outer cells at the moment of full compaction. Recently Zhu et al. (Zhu *et*
420 *al.*, 2021) revealed that in human embryos polarity occurs in two steps: first F-actin is
421 concentrated at the cell-contact free surface, followed by PAR6/PKC apical cap

422 polarity. Here we demonstrated that this process is preceded by p-ERM polarity, most
423 likely to link F-actin to the plasma membrane, and we suggest that the apical cap in
424 compacted human embryos is established in three steps: first p-ERM, followed by F-
425 actin and finally the PAR complex proteins. Co-localisation of p-ERM, F-actin, PAR6
426 and aPKC proteins points to maturation of the apical cap when compaction is
427 completed and blastulation starts.
428 In human embryos, the first lineage differentiation is orchestrated by polarity and YAP1
429 and GATA3 co-localisation in the compacted embryo (Gerri *et al.*, 2020). By carefully
430 examining YAP1/GATA3 co-staining at different stages of development, we observed
431 that YAP1 and GATA3 co-localise in a significant number of nuclei in the
432 compacting/polarising human embryo before inner and outer cells are established and
433 before the apical cap is formed while we never observed GATA3+/YAP1- nuclei
434 throughout compaction. This strongly supports the causal relationship between YAP1
435 presence and *GATA3* expression (Gerri *et al.*, 2020; Zhu *et al.*, 2021). We propose, as
436 also suggested by Zhu et al. (Zhu *et al.*, 2021), that *YAP1* expression can be initiated
437 independently of polarity. *YAP1* expression could be induced by other mechanisms
438 such as cell-cell contact and/or contractility since YAP1 is very sensitive to mechanical
439 cues (Maître *et al.*, 2015; Maître, 2017). We propose that the apical cap reinforces TE
440 initiation, as also suggested by Zhu et al. (Zhu *et al.*, 2021). This does not exclude that
441 in polarizing cells *YAP1* expression is initiated by the polarisation process, which is an
442 ongoing process that is finalized when polarity is fully established, or that *YAP1* is
443 induced by polarity in polarized cells, but this can only be investigated further by live
444 imaging.
445 In contrast to previous imaging studies in mouse compacted 16-cell stage embryos
446 where non-polarized cells are frequently found on the outside (Anani *et al.*, 2014), we
447 did not observe non-polarized cells in an outer position in compacted human embryos.
448 In mouse embryos, these non-polarized cells are actively sorted into an inner position
449 and assume the ICM fate. We did not detect polarized cells in an inner position in
450 compacted human embryos, as reported in mouse embryos (Anani *et al.*, 2014),
451 however we found YAP1 positive cells in an inner position (25%). Misallocated cells
452 could be sorted to the correct position (Zhu *et al.*, 2021). or could change lineage
453 direction due to plasticity. On some occasions, we found YAP1 and GATA3 co-
454 localized in ICM (5 dpf) and PrE (6 dpf) cells, where they most likely originate from
455 miss-positioning during compaction and early blastulation.

456 In human embryos, YAP1, TEAD1 and TEAD4 are present in the nuclei before
457 compaction and polarity are completely established, as described in the mouse but
458 their role is unknown. YAP1 and TEAD4 proteins were found to play a role in EGA in
459 mouse embryos (Yu *et al.*, 2016; Sha *et al.*, 2020) and together with TFAP2C and
460 RhoA, TEAD4 was found to play a crucial role in apical domain formation in mice (Zhu
461 *et al.*, 2020), but this has not yet been investigated in humans. The upstream signals
462 inducing YAP1, TEAD1 and TEAD4 expression in human and mouse embryos are
463 unknown.
464 We found that TEAD1, which is present in all the blastomeres during
465 compaction, precedes TEAD4. Since TEAD4 is ubiquitously present from the
466 compacted embryos stage onwards while TEAD1/YAP1 are differentially co-localised
467 in what we propose to be (precursor-) TE and PrE cells, we suggest that TEAD1 rather
468 than TEAD4 is involved in the segregation of the TE and PrE lineages in humans.
469 Our data point to differences in the first lineage differentiation event between
470 mice and humans. In the mouse, differentiation into TE and ICM cells is known to be
471 orchestrated by cell polarity, contractility and TEAD4/YAP1 interaction (Nishioka *et al.*,
472 2008, 2009; Ralston *et al.*, 2010; Hirate and Sasaki, 2014; Maître *et al.*, 2015; Maître,
473 2017). Complete compaction and polarity are promptly established at the 8-cell stage.
474 When dividing from the 8- to the 16-cell stage, symmetric and asymmetric divisions
475 determine the blastomeres' fate.
476 Like in many other mammalian species including the bovine, human embryos do not
477 pass through a stage where all blastomeres are polarized (Pfeffer, 2018). Polarisation,
478 compaction and establishment of inner and outer cells appear to happen gradually and
479 simultaneously while dividing from 8 to 16 cells. Our data supports also the conclusion
480 that there are no symmetric and asymmetric divisions when the human embryo divides
481 from 8 to 16 cells since 8-cell stage blastomeres are not polarized. We confirmed this
482 by analysing the divisions in isolated human 8-cell stage blastomeres and detected
483 two patterns. It is tempting to speculate that these patterns I and II represent
484 asymmetric and symmetric divisions, respectively, however within one embryo all
485 blastomeres follow the same pattern. By time lapse kinetics we demonstrated that
486 pattern I corresponds with the normal kinetics of compaction and cavitation during
487 human pre-implantation development and pattern II development is delayed and
488 therefore abnormal. Currently, we do not know how one of the two cells in the 2/16
489 couplets becomes polarized, we propose that the 8-cell stage blastomeres are

490 plenipotent (Condic, 2014; Krivega *et al.*, 2015). After the fourth round of mitotic
491 divisions the lineage direction of the 16-cell stage blastomeres in the embryo could be
492 determined by polarity, position, contact, cortical tension and/or the Hippo signalling
493 pathway; this could be different in compacted 8-cell stage embryos and non-
494 compacted 16-cell stage human embryos. Interestingly, the polarity model with
495 symmetric and asymmetric divisions in mouse embryos has been recently challenged
496 using live YAP1 imaging (Gu *et al.*, 2022). Apparently at the 8- and 16-cell stages all
497 blastomeres display nuclear YAP1, but it is rapidly downregulated in the inner cells of
498 the compacted mouse embryo. Live staining on human embryos is extremely
499 challenging, but if this could be confirmed in human embryos the first lineage
500 differentiation event in the mouse and the human may be more similar than currently
501 thought. Recently, after *TEAD4* depletion by CRISPR/Cas9 in human zygotes it was
502 found that blastocysts are formed and *CDX2* expression but not *GATA3* expression is
503 downregulated, providing evidence that TEAD4/YAP1 signalling plays a role in the
504 maintenance rather than initiation of TE lineage differentiation (Stamatiadis *et al.*,
505 2022). We suggest that in the compacted human embryo TEAD1/YAP1/GATA3 co-
506 localisation in the outer cells initiates TE lineage differentiation; in inner cells TEAD1,
507 YAP1 and GATA3 do not co-localize and these cells remain pluripotent.

508 We also demonstrate that the second lineage differentiation event occurs
509 differently in humans and mice. In the human embryo, the lineages arising during the
510 second differentiation have been described by immunostainings, but the signalling
511 pathways initiating and maintaining the lineages have not been found yet. GATA6
512 proteins are present in the nuclei of all the blastomeres after EGA and become
513 restricted in PrE cells when SOX17 and GATA4 are upregulated, in salt-and-pepper
514 pattern and segregation into inner EPI cells and PrE cells facing the cavity (Kimber *et*
515 *al.*, 2008; Kuijk *et al.*, 2012; Roode *et al.*, 2012; Niakan and Eggan, 2013). Here we
516 showed that in human blastocysts the PrE lineage is characterized by the co-
517 localisation of TEAD1 and YAP1. Since the PrE specific markers GATA4 and SOX17
518 can appear in the absence of TEAD1/YAP1 co-localisation, we suggest that the
519 interaction maintains the PrE lineage rather than initiating it. This is different from the
520 mouse model where TEAD/YAP1 interaction orchestrates the expression of *Sox2*
521 (Wicklow *et al.*, 2014) and differentiation into the EPI lineage (Hashimoto and Sasaki,
522 2019). After carefully counting cells expressing NANOG, SOX17 and/or GATA4, we
523 found that on 5 dpf in the majority of the B3 blastocysts nuclear NANOG is found in all

524 the ICM cells. In B3 embryos the EPI/PrE-markers co-localize in a small population of
525 the ICM cells (6.2%). On 6 dpf, 2/3 of the ICM cells are EPI cells while 1/3 of the inner
526 cells are PrE cells. According to our data the human TE, EPI and PrE lineages do not
527 emerge simultaneously (Petropoulos, 2016), but in two steps (Meistermann *et al.*,
528 2021). Our data also support the hypothesis that PrE cells differentiate from EPI cells
529 in expanding blastocysts (between B3 on 5 dpf and B4 on 6 dpf) (Meistermann *et al.*,
530 2021). Their single-cell transcriptomics data and our NANOG analysis also suggest
531 that the ICM (5 dpf) and EPI (6 dpf) are very similar (if not the same), but further
532 characterization of the pluripotent cells is needed to precisely define the stages
533 (Radley et al., 2022).
534 We conclude that the TE and PrE lineage differentiation events in human
535 embryos is specified by TEAD1 and YAP1 co-localisation. This study establishes a
536 detailed roadmap on polarisation, compaction, position and lineage segregation during
537 human pre-implantation development paving the road for further functional studies.
538

539 **Material and Methods**

540

541 **Ethical statement**

542 This project was approved by the Local Ethical Committee of the UZ Brussel (BUN
543 143201526417) and the Belgian Federal Committee for research on human embryos
544 (AdV057). We used cryopreserved human embryos donated to research from IVF-ICSI
545 patients after informed consent and the expiration of the 5-year cryopreservation
546 duration. Mature oocytes were obtained from egg bank donors who voluntary donated
547 gametes for research.

548

549 **Embryo warming and culture**

550 Human vitrified high quality 8-cell stage human embryos (3 dpf) were warmed (Vit Kit
551 -Thaw, Irvine Scientific, USA) and cultured until 6 dpf in individual microdroplets of 25µl
552 medium (Quinn's Advantage™ Blastocyst media, Origio, USA) under a layer of paraffin
553 oil (OVOIL™ - culture oil, Vitrolife, USA) to prevent evaporation of medium. Embryos
554 were incubated at 37°C, 5% O2 and 6% CO2 tension. Warmed embryos were scored
555 for viability per blastomere after warming, overall survival of the embryos was at 99%.
556 Embryos with signs of degeneration in more than one cell were excluded as well as
557 embryos that showed more than 10% fragmentation, with irregular size of blastomeres,
558 increased amounts of vacuoles or granulation and arrested embryos.

559

560 **Developmental timeline of the human embryo**

561 The embryos were scored according to their developmental stage displaying
562 morphological key differences rather than defining them according to their
563 chronological age (dpf) (Supplementary Table 1). The compaction process was divided
564 into three subgroups. At the beginning of compaction (C0) the outlines of the individual
565 blastomeres within the embryo were clearly visible. However, the cell shape appeared
566 slightly elongated. Shortly after, intercellular contacts increased due to adherence
567 junctions (C1). At the end of compaction (C2) the blastomeres had maximized their
568 contact sites and the embryo appeared as a sphere of contour-less tightly packed cells.
569 The blastulation process was divided into four subgroups. Transition from the fully
570 compacted embryo to the early blastocyst stage (B0) was marked by a slight
571 decompaction as cellular outlines were once again visible, small cavities were formed
572 and sickle-cell shaped outer cells became apparent. Subsequently one cavity was

573 formed (B1). As soon as the ICM was visible, the outer cells were referred to as TE in
574 a full blastocyst (B2). As fluid accumulated further the embryo started to expand as an
575 increase in size could be observed due to TE cell proliferation and ZP thinning (B3).
576 Subsequently the blastocyst expanded (B4) and started to hatch out of the ZP (B5)
577 until it was fully hatched (B6).
578
579 **Immunofluorescence**
580 Cultured embryos were fixed in 4% PFA/PBS for 10 minutes at room temperature (RT)
581 to crosslink proteins and preserve cellular integrity. After fixation embryos were
582 washed three times for 10 minutes in 2% BSA/PBS before permeabilization of
583 membranes in 0,1% TritonX/PBS for 20 minutes at RT to increase access for antibody
584 binding. Subsequently embryos were placed in 10% FBS/PBS blocking solution for 1h
585 at RT to decrease unspecific antibody binding before incubation with primary antibody
586 or control-IgG antibody (Supplementary Table 2) in 2% FBS/BSA overnight at 4°C.
587 Embryos were washed in 2% BSA/PBS before incubation with secondary antibody
588 (Supplementary Table 2) at 10 µg/ml for 2h at RT in the dark, after 1h of secondary
589 antibody incubation fluorochrome conjugated phalloidin (Alexa Fluor™ 546 Phalloidin,
590 Invitrogen™) was added to the secondary antibody solution for F-actin membrane
591 staining for another hour. Embryos were washed again in 2% BSA/PBS before
592 incubation with Hoechst 33342 (Molecular probes®, Life Technologies) for nuclear
593 staining. Eventually embryos were mounted in 1xPBS on poly -L-lysine coated glass
594 slides (Poly-Prep Slides, Sigma-Aldrich) to prevent collapse and movement during
595 visualization. Round coverslips were sandwiched between the glass slide and the
596 coverslip (Corning® Cover Glasses, #1.5, Sigma-Aldrich) and glued together with nail
597 polish to prevent squeezing of the embryo.
598
599 **Confocal microscopy and visualisation**
600 Fluorescence of immunostained embryos was detected with a confocal microscope
601 (LSM800 equipped with Airyscan, ZEISS). Whole embryo z-stack scans were carried
602 out to reconstruct the 3D anatomy of the embryo. To omit spectral overlap between
603 fluorophores, emission filters for each fluorophore were employed. Z-stacks were
604 processed with the Zen-Blue software (ZEISS) and image sequences were exported
605 and analysed for cell counts with ImageJ and Arivis Vision 4D (3.4.0). The number of
606 nuclei (positive for DNA) was assessed using the Blob finder function of Arivis. All other

607 counts were assessed manually. We considered a nucleus positive for a protein when
608 the signal visibly exceeded the background and/or when the signal was clearly
609 delineated from the cytoplasm. We confirmed our manual approach by measuring
610 fluorescence intensities of YAP1 and GATA3 at the earlier stages when signals started
611 to emerge, thus when weak signals are more prone to operator error (Fig. 4B) using
612 the 3D Fiji/Image J Suite as previously described (Gerri *et al.*, 2020, 2022).
613
614 **Micromanipulation**
615 Warmed 8-cell stage human embryos without any sign of fragmentation were split by
616 micromanipulation into eight single blastomeres as described (van de Velde *et al.*,
617 2008) and cultured until dpf6 and fixed for immunostainings as described above.
618
619 **Statistics**
620 Statistics on compaction and cavitation times (Fig. 5E-G) were using permutation
621 testing with 10000 permutations of our data. A two-tailed p-value was determined by
622 (2*(sum(results) > mean difference)/10000)). We used a two tailed Mann Whitney U
623 test for the data regarding the fluorescence intensities (Fig. 4B). All graphs and
624 statistics were generated using GraphPad Prism (9.0.0.) and R-Studio (1.1.456).
625

626 **Author contributions**

627 MR experiments, interpretation, writing, editing, final approval

628 WE experiments, interpretation, writing, editing, final approval

629 AD experiments, interpretation, final approval

630 DD experiments, editing, final approval

631 LD interpretation, editing, final approval

632 CG interpretation, editing, final approval

633 KN interpretation, editing, final approval

634 GV editing, final approval

635 HT editing, final approval

636 JS experiments, editing, final approval

637 KS interpretation, writing, editing, final approval

638 HVdV study design, interpretation, writing, editing, final approval

639

640 **Competing interests**

641 The authors declare no competing interests.

642

643 **Acknowledgements**

644 We thank Wilfried Cools from the Biostatistics and Medical Informatics Group (VUB)
645 for the statistical advice. This work was financially supported by Wetenschappelijk
646 Fonds Willy Gepts (WFWG) of the University Hospital UZ Brussel. M.R. is doctoral
647 fellow at the Fonds Wetenschappelijk Onderzoek – Vlaanderen (FWO).

648

649

650 **References**

651 Alarcon, V.B. (2010) 'Cell polarity regulator PARD6B is essential for trophectoderm
652 formation in the preimplantation mouse embryo', *Biology of reproduction*, 83(3), pp.
653 347–358. Available at: https://doi.org/10.1095/BIOLREPROD.110.084400.
654
655 Anani, S. *et al.* (2014) 'Initiation of Hippo signaling is linked to polarity rather than to
656 cell position in the pre-implantation mouse embryo', *Development (Cambridge,*
657 *England)*, 141(14), pp. 2813–2824. Available at: https://doi.org/10.1242/DEV.107276.
658
659 Blakeley, P. *et al.* (2015) 'Defining the three cell lineages of the human blastocyst by
660 single-cell RNA-seq', *Development (Cambridge, England)*, 142(18), pp. 3151–3165.
661 Available at: https://doi.org/10.1242/DEV.123547.
662
663 Chazaud, C. *et al.* (2006) 'Early lineage segregation between epiblast and primitive
664 endoderm in mouse blastocysts through the Grb2-MAPK pathway', *Developmental*
665 *cell*, 10(5), pp. 615–624. Available at: https://doi.org/10.1016/J.DEVCEL.2006.02.020.
666
667 Chazaud, C. and Yamanaka, Y. (2016) 'Lineage specification in the mouse
668 preimplantation embryo', *Development*, 143(7), pp. 1063–1074. Available at:
669 https://doi.org/10.1242/DEV.128314.
670
671 Condic, M.L. (2014) 'Totipotency: What it is and what it is not', *Stem Cells and*
672 *Development*. Mary Ann Liebert Inc., pp. 796–812. Available at:
673 https://doi.org/10.1089/scd.2013.0364.
674
675 Dietrich, J.E. and Hiiragi, T. (2007) 'Stochastic patterning in the mouse pre-
676 implantation embryo', *Development (Cambridge, England)*, 134(23), pp. 4219–4231.
677 Available at: https://doi.org/10.1242/DEV.003798.
678
679 Gerri, C. *et al.* (2020) 'Initiation of a conserved trophectoderm program in human, cow
680 and mouse embryos', *Nature*, 587(7834), pp. 443–447. Available at:
681 https://doi.org/10.1038/S41586-020-2759-X.
682

683 Gerri, C. *et al.* (2022) 'A conserved role of Hippo signaling in initiation of the first lineage
684 specification event across mammals', *bioRxiv*, p. 2022.07.01.498418. Available at:
685 https://doi.org/10.1101/2022.07.01.498418.
686
687 Gu, B. *et al.* (2022) 'Live imaging YAP signalling in mouse embryo development', *Open*
688 *Biology*, 12(1). Available at: https://doi.org/10.1098/RSOB.210335.
689
690 Harada, Y. *et al.* (2020) 'Selection of high-quality and viable blastocysts based on
691 timing of morula compaction and blastocyst formation', *Reproductive Medicine and*
692 *Biology*, 19(1), p. 58. Available at: https://doi.org/10.1002/RMB2.12302.
693
694 Hashimoto, M. and Sasaki, H. (2019) 'Epiblast Formation by TEAD-YAP-Dependent
695 Expression of Pluripotency Factors and Competitive Elimination of Unspecified Cells',
696 *Developmental cell*, 50(2), pp. 139-154.e5. Available at:
697 https://doi.org/10.1016/J.DEVCEL.2019.05.024.
698 Hirate, Y. and Sasaki, H. (2014) 'The role of angiomotin phosphorylation in the Hippo
699 pathway during preimplantation mouse development', *Tissue barriers*, 2(1). Available
700 at: https://doi.org/10.4161/TISB.28127.
701
702 Iwata, K. *et al.* (2014) 'Analysis of compaction initiation in human embryos by using
703 time-lapse cinematography', *Journal of Assisted Reproduction and Genetics*, 31(4), p.
704 421. Available at: https://doi.org/10.1007/S10815-014-0195-2.
705
706 Johnson, M.H. and Ziomek, C.A. (1981) 'The foundation of two distinct cell lineages
707 within the mouse morula', *Cell*, 24(1), pp. 71–80. Available at:
708 https://doi.org/10.1016/0092-8674(81)90502-X.
709
710 Kimber, S.J. *et al.* (2008) 'Expression of genes involved in early cell fate decisions in
711 human embryos and their regulation by growth factors', *Reproduction*, 135(5), pp. 635–
712 647. Available at: https://doi.org/10.1530/REP-07-0359.
713
714 Krivega, M. v. *et al.* (2015) 'Cyclin E1 plays a key role in balancing between totipotency
715 and differentiation in human embryonic cells', *Molecular Human Reproduction*, 21(12),
716 pp. 942–956. Available at: https://doi.org/10.1093/molehr/gav053.

717
718 Kuijk, E.W. *et al.* (2012) 'The roles of FGF and MAP kinase signaling in the segregation
719 of the epiblast and hypoblast cell lineages in bovine and human embryos',
720 *Development (Cambridge, England)*, 139(5), pp. 871–882. Available at:
721 https://doi.org/10.1242/DEV.071688.
722
723 Levy, J.B. *et al.* (1986) 'The timing of compaction: control of a major developmental
724 transition in mouse early embryogenesis', *Development*, 95(1), pp. 213–237. Available
725 at: https://doi.org/10.1242/DEV.95.1.213.
726
727 Lorthongpanich, C. *et al.* (2012) 'Developmental fate and lineage commitment of
728 singled mouse blastomeres', *Development*, 139(20), pp. 3722–3731. Available at:
729 https://doi.org/10.1242/DEV.086454.
730
731 Lorthongpanich, C. and Issaragrisil, S. (2015) 'Emerging Role of the Hippo Signaling
732 Pathway in Position Sensing and Lineage Specification in Mammalian Preimplantation
733 Embryos', *Biology of reproduction*, 92(6). Available at:
734 https://doi.org/10.1095/BIOLREPROD.114.127803.
735
736 Maître, J.L. *et al.* (2015) 'Pulsatile cell-autonomous contractility drives compaction in
737 the mouse embryo', *Nature cell biology*, 17(7), pp. 849–855. Available at:
738 https://doi.org/10.1038/NCB3185.
739
740 Maître, J.L. (2017) 'Mechanics of blastocyst morphogenesis', *Biology of the Cell*,
741 109(9), pp. 323–338. Available at: https://doi.org/10.1111/BOC.201700029.
742
743 Meistermann, D. *et al.* (2021) 'Integrated pseudotime analysis of human pre-
744 implantation embryo single-cell transcriptomes reveals the dynamics of lineage
745 specification', *Cell Stem Cell*, 28(9), pp. 1625-1640.e6. Available at:
746 https://doi.org/10.1016/j.stem.2021.04.027.
747 Motato, Y. *et al.* (2016) 'Morphokinetic analysis and embryonic prediction for blastocyst
748 formation through an integrated time-lapse system', *Fertility and Sterility*, 105(2), pp.
749 376-384.e9. Available at: https://doi.org/10.1016/j.fertnstert.2015.11.001.
750

751 Niakan, K.K. and Eggan, K. (2013) 'Analysis of human embryos from zygote to
752 blastocyst reveals distinct gene expression patterns relative to the mouse',
753 *Developmental biology*, 375(1), pp. 54–64. Available at:
754 https://doi.org/10.1016/J.YDBIO.2012.12.008.
755
756 Nishioka, N. *et al.* (2008) 'Tead4 is required for specification of trophectoderm in pre-
757 implantation mouse embryos', *Mechanisms of development*, 125(3–4), pp. 270–283.
758 Available at: https://doi.org/10.1016/J.MOD.2007.11.002.
759
760 Nishioka, N. *et al.* (2009) 'The Hippo Signaling Pathway Components Lats and Yap
761 Pattern Tead4 Activity to Distinguish Mouse Trophectoderm from Inner Cell Mass',
762 *Developmental Cell*, 16(3), pp. 398–410. Available at:
763 https://doi.org/10.1016/J.DEVCEL.2009.02.003.
764
765 Petropoulos, S. (2016) 'Single-cell RNA-seq reveals lineage and X chromosome
766 dynamics in human preimplantation embryos', *Cell*, 165, pp. 1012–1026.
767
768 Pfeffer, P.L. (2018) 'Building Principles for Constructing a Mammalian Blastocyst
769 Embryo', *Biology 2018, Vol. 7, Page 41*, 7(3), p. 41. Available at:
770 https://doi.org/10.3390/BIOLOGY7030041.
771
772 Plusa, B. *et al.* (2005) 'Downregulation of Par3 and aPKC function directs cells towards
773 the ICM in the preimplantation mouse embryo', *Journal of cell science*, 118(Pt 3), pp.
774 505–515. Available at: https://doi.org/10.1242/JCS.01666.
775
776 Radley, A. *et al.* (2022) 'Entropy sorting of single cell RNA sequencing data reveals
777 the inner cell mass in the human pre-implantation embryo', *bioRxiv*, p.
778 2022.04.08.487653. Available at: https://doi.org/10.1101/2022.04.08.487653.
779
780 Radley, A., Smith, A. and Dunn, S.-J. (2022) 'Functional feature selection reveals the
781 inner cell mass in human pre-implantation embryo single cell RNA sequencing data',
782 *bioRxiv*, p. 2022.04.08.487653. Available at:
783 https://doi.org/10.1101/2022.04.08.487653.
784

785 Ralston, A. *et al.* (2010) 'Gata3 regulates trophoblast development downstream of
786 Tead4 and in parallel to Cdx2', *Development (Cambridge, England)*, 137(3), pp. 395–
787 403. Available at: https://doi.org/10.1242/DEV.038828.
788
789 Rienzi, L. *et al.* (2019) 'Time of morulation and trophectoderm quality are predictors of
790 a live birth after euploid blastocyst transfer: a multicenter study', *Fertility and Sterility*,
791 112(6), pp. 1080-1093.e1. Available at:
792 https://doi.org/10.1016/J.FERTNSTERT.2019.07.1322/ATTACHMENT/8A49BAC8-
793 8762-4F98-BF30-20F642936EC3/MMC2.DOCX.
794
795 Roode, M. *et al.* (2012) 'Human hypoblast formation is not dependent on FGF
796 signalling', *Developmental Biology*, 361(2–6), p. 358. Available at:
797 https://doi.org/10.1016/J.YDBIO.2011.10.030.
798 Sha, Q.Q. *et al.* (2020) 'Dynamics and clinical relevance of maternal mRNA clearance
799 during the oocyte-to-embryo transition in humans', *Nature Communications 2020 11:1*,
800 11(1), pp. 1–16. Available at: https://doi.org/10.1038/s41467-020-18680-6.
801
802 Skiadas, C.C., Jackson, K. v. and Racowsky, C. (2006) 'Early compaction on day 3
803 may be associated with increased implantation potential', *Fertility and sterility*, 86(5),
804 pp. 1386–1391. Available at: https://doi.org/10.1016/J.FERTNSTERT.2006.03.051.
805
806 Stamatiadis, P. *et al.* (2022) 'TEAD4 regulates trophectoderm differentiation upstream
807 of CDX2 in a GATA3 -independent manner in the human preimplantation embryo',
808 *Human Reproduction* [Preprint]. Available at:
809 https://doi.org/10.1093/HUMREP/DEAC138.
810
811 Stirparo, G.G. *et al.* (2018) 'Integrated analysis of single-cell embryo data yields a
812 unified transcriptome signature for the human pre-implantation epiblast', *Development*
813 *(Cambridge, England)*, 145(3). Available at: https://doi.org/10.1242/DEV.158501.
814
815 van de Velde, H. *et al.* (2008) 'The four blastomeres of a 4-cell stage human embryo
816 are able to develop individually into blastocysts with inner cell mass and
817 trophectoderm', *Human reproduction (Oxford, England)*, 23(8), pp. 1742–1747.
818 Available at: https://doi.org/10.1093/HUMREP/DEN190.

819

820 Wicklow, E. *et al.* (2014) 'HIPPO Pathway Members Restrict SOX2 to the Inner Cell
821 Mass Where It Promotes ICM Fates in the Mouse Blastocyst', *PLOS Genetics*, 10(10),
822 p. e1004618. Available at: https://doi.org/10.1371/JOURNAL.PGEN.1004618.
823

824 Yamanaka, Y., Lanner, F. and Rossant, J. (2010) 'FGF signal-dependent segregation
825 of primitive endoderm and epiblast in the mouse blastocyst', *Development (Cambridge,*
826 *England)*, 137(5), pp. 715–724. Available at: https://doi.org/10.1242/DEV.043471.
827

828 Yan, L. *et al.* (2013) 'Single-cell RNA-Seq profiling of human preimplantation embryos
829 and embryonic stem cells', *Nature Structural & Molecular Biology*, 20(9), pp. 1131–
830 1139. Available at: https://doi.org/10.1038/nsmb.2660.
831

832 Yu, C. *et al.* (2016) 'Oocyte-expressed yes-associated protein is a key activator of the
833 early zygotic genome in mouse', *Cell research*, 26(3), pp. 275–287. Available at:
834 https://doi.org/10.1038/CR.2016.20.
835

836 Zhu, M. *et al.* (2017) 'Actomyosin polarisation through PLC-PKC triggers symmetry
837 breaking of the mouse embryo', *Nature Communications 2017 8:1*, 8(1), pp. 1–16.
838 Available at: https://doi.org/10.1038/s41467-017-00977-8.
839

840 Zhu, M. *et al.* (2020) 'Developmental clock and mechanism of de novo polarization of
841 the mouse embryo', *Science (New York, N.Y.)*, 370(6522). Available at:
842 https://doi.org/10.1126/SCIENCE.ABD2703.
843

844 Zhu, M. *et al.* (2021) 'Human embryo polarization requires PLC signaling to mediate
845 trophectoderm specification', *eLife*, 10. Available at:
846 https://doi.org/10.7554/ELIFE.65068.
847

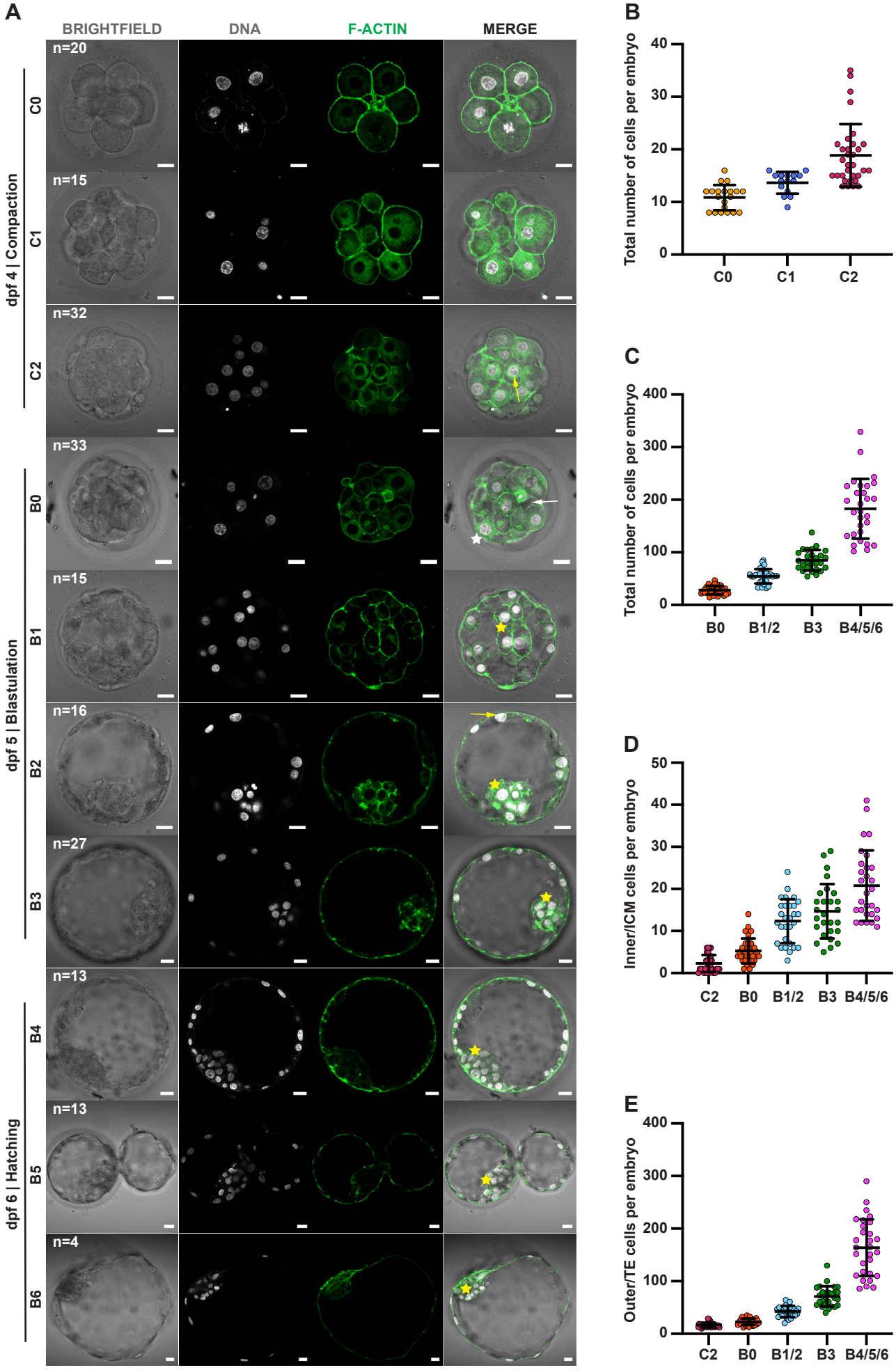
A
BRIGHTFIELD
DNA
F-ACTIN
MERGE
dpf 4 | Compaction
C0
C1
C2
dpf 5 | Blastulation
B0
B1
B2
B3
dpf 6 | Hatching
B4
B5
B6
n=20
n=15
n=32
n=33
n=15
n=16
n=27
n=13
n=13
n=4
B
Total number of cells per embryo
C0
C1
C2
C
Total number of cells per embryo
B0
B1/2
B3
B4/5/6
D
Inner/ICM cells per embryo
C2
B0
B1/2
B3
B4/5/6
E
Outer/TE cells per embryo
C2
B0
B1/2
B3
B4/5/6

Figure 1: Inner and outer cells are established in the compacted human embryo

(A) Developmental timeline of the human embryo based on morphology (Brightfield) and distribution of F-actin (green) and DNA (white) at 4 days post fertilisation (dpf) (C0-C2), 5 dpf (B0-B3) and 6 dpf (B4-B6). At the beginning of compaction (C0) the contact between de blastomeres increases and the cell shape appears slightly elongated, but the outlines of the individual blastomeres within the embryo are still clearly visible. Shortly after, the cellular borders begin to fade as a result of increased intercellular contacts due to adherence junctions and the embryo is compacting (C1). When compaction is completed (C2) the blastomeres have maximized their contact sites and the embryo appears as a sphere of contour-less tightly packed cells. During this stage the first inner cells (yellow arrow) appear. The initiation of blastulation (B0) is marked by a slight decompaction (white arrow) as cellular outlines are once again visible and the outer cells become sickle-cell shaped (white star) and the cavity is formed (B1). As soon as the ICM (B2-B6, yellow stars) is visible, the outer cells are referred to as trophectoderm (TE) cells (yellow arrow). During the B3 stage, the blastocyst expands with coinciding zona pellucida thinning. In addition, at 6 dpf an increase in blastocyst size can be observed due to TE cell proliferation (B4). Subsequently the blastocyst starts to hatch (B5) until fully hatched out of the ZP (B6).

(B) Total number of cells per embryo during compaction (C0-C2).

Brightfield images were taken after fixation. Scale bars, 20µm. All error bars are mean ± SD.

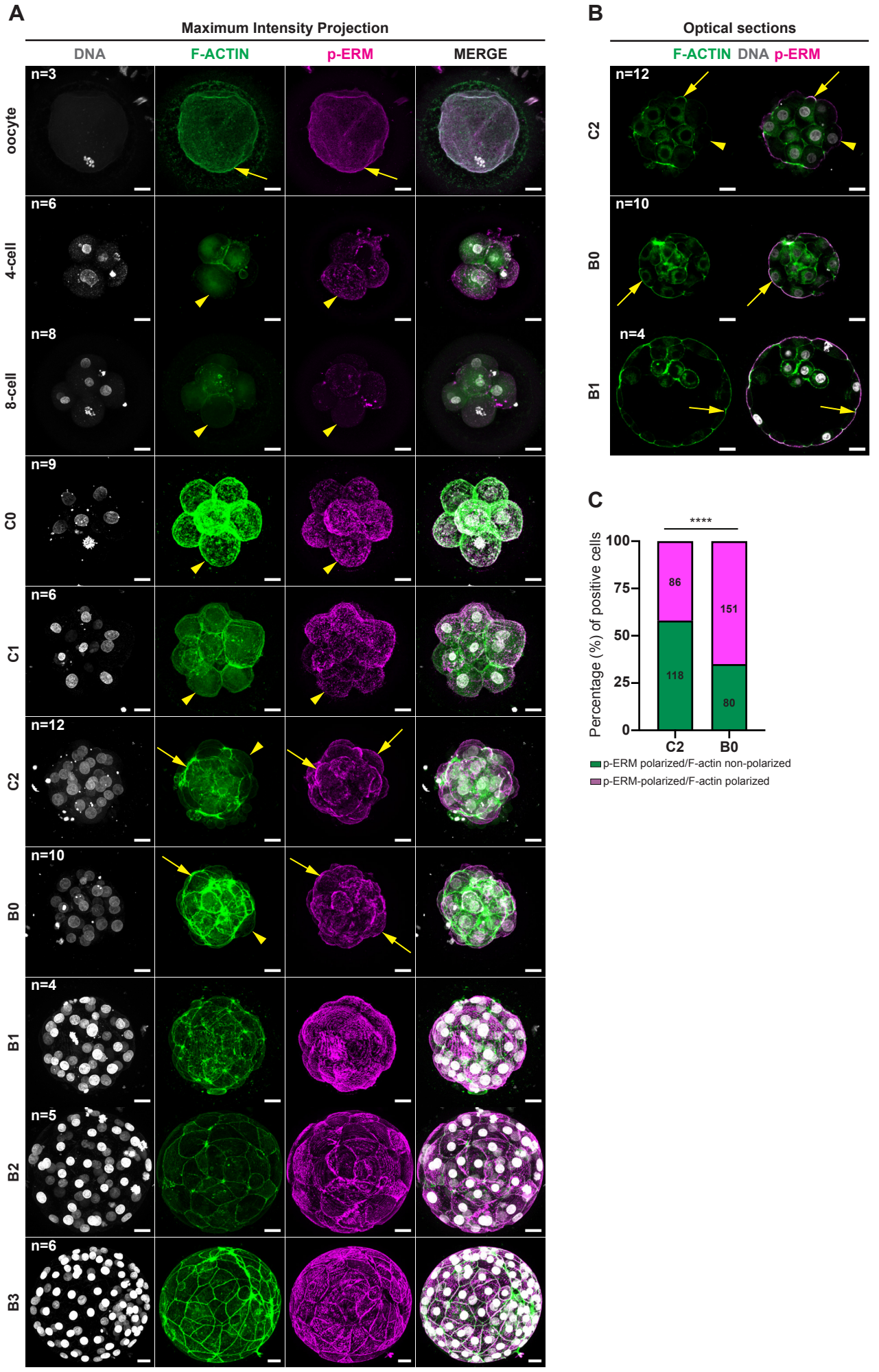
A
Maximum Intensity Projection
DNA
F-ACTIN
p-ERM
MERGE
oocyte
4-cell
8-cell
C0
C1
C2
B0
B1
B2
B3
n=3
n=6
n=8
n=9
n=6
n=12
n=10
n=4
n=5
n=6
B
Optical sections
F-ACTIN DNA p-ERM
C2
B0
B1
n=12
n=10
n=4
C
****
Percentage (%) of positive cells
100
75
50
25
0
86
151
118
80
C2
B0
p-ERM polarized/F-actin non-polarized
p-ERM-polarized/F-actin polarized

Figure 2: P-ERM apical polarity proceeds F-actin apical polarity in the compacted human embryo

(A) Maximum intensity projections of different developmental stages analysed for DNA (white), F-actin (green) and p-ERM (magenta). Presence of F-actin and p-ERM apical polarity (yellow arrows); absence of apical polarity (yellow arrow heads).

(B) Optical section of embryos (C2, B0, B1) analysed for F-actin (green), DNA (white) and p-ERM (magenta). F-actin apical polarity indicated by yellow arrow, absence indicated by yellow arrowheads.

(C) Percentage of positive cells at the C2 and B0 stage that show either p-ERM and F-actin polarisation or p-ERM polarisation without F-actin (****$p<0.00001$, Fisher-exact-test).

Brightfield images were taken before fixation. Scale bars, 20µm.

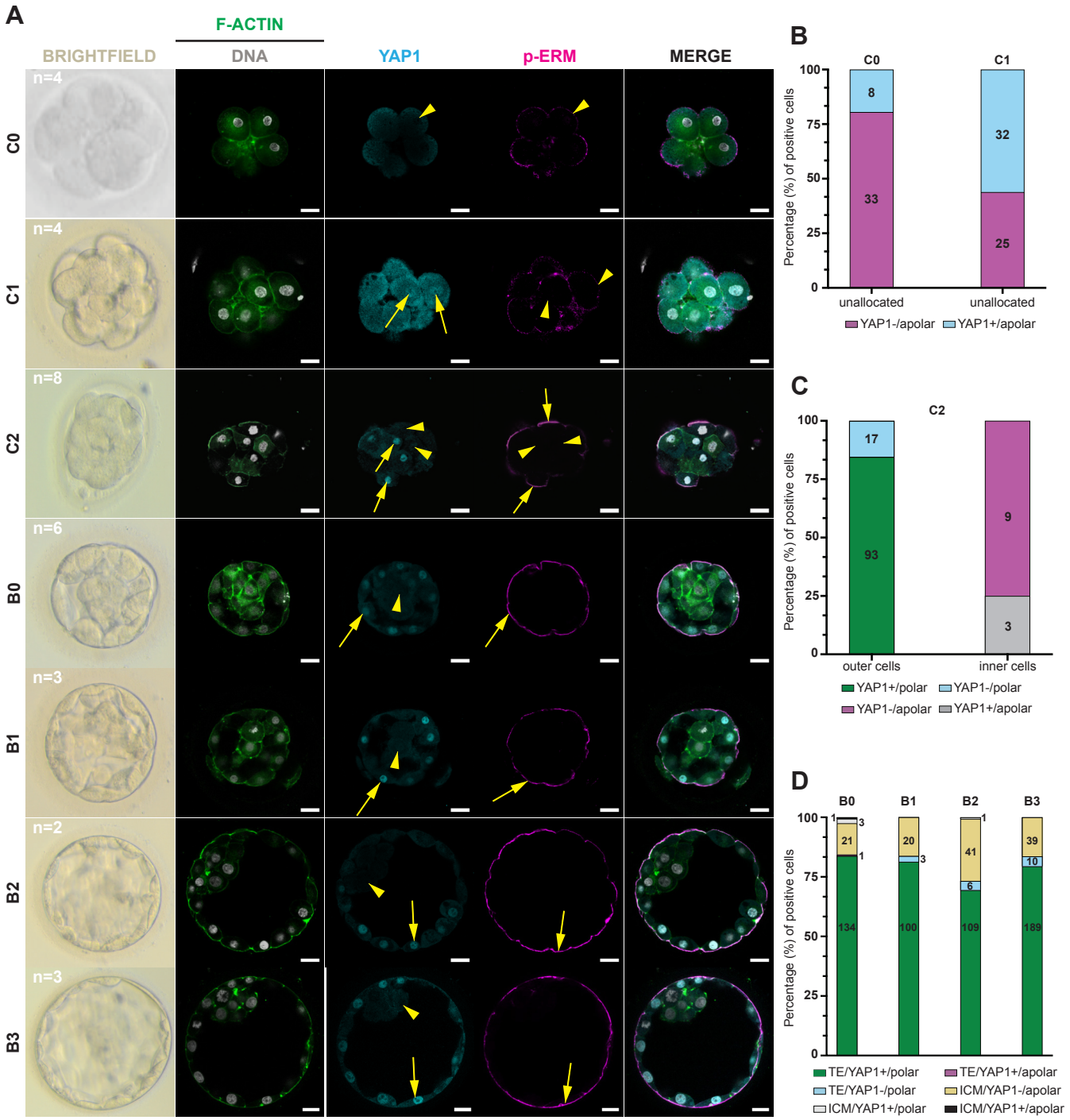
A
F-ACTIN
BRIGHTFIELD
DNA
YAP1
p-ERM
MERGE
C0
C1
C2
B0
B1
B2
B3
n=4
n=4
n=8
n=6
n=3
n=2
n=3
B
C0
C1
Percentage (%) of positive cells
8
33
32
25
unallocated
unallocated
YAP1-/apolar
YAP1+/apolar
C
C2
17
93
9
3
outer cells
inner cells
YAP1+/polar
YAP1-/polar
YAP1-/apolar
YAP1+/apolar
D
B0
B1
B2
B3
1
3
21
1
134
20
3
100
1
41
6
109
39
10
189
TE/YAP1+/polar
TE/YAP1+/apolar
TE/YAP1-/polar
ICM/YAP1-/apolar
ICM/YAP1+/polar
ICM/YAP1+/apolar

Figure 3: YAP1 expression becomes mainly restricted to polar outer cells from the compacted human embryo stage onwards

(A) Optical sections of embryos (C0-B3) analysed for DNA (white), F-actin (green), YAP1 (turquoise) and p-ERM (magenta), presence indicated by yellow arrow, absence indicated by yellow arrowheads.
(B) Percentage of apolar cells positive or negative for YAP1 during C0 and C1 stages.
(C) Percentage of YAP1 positive/negative cells in polar/apolar outer and inner cells of C2 embryos.
(D) Percentage of TE and ICM cells of B0-B3 embryos positive/negative for YAP1 and polar/apolar.
Brightfield images were taken before fixation. Scale bars, 20µm.

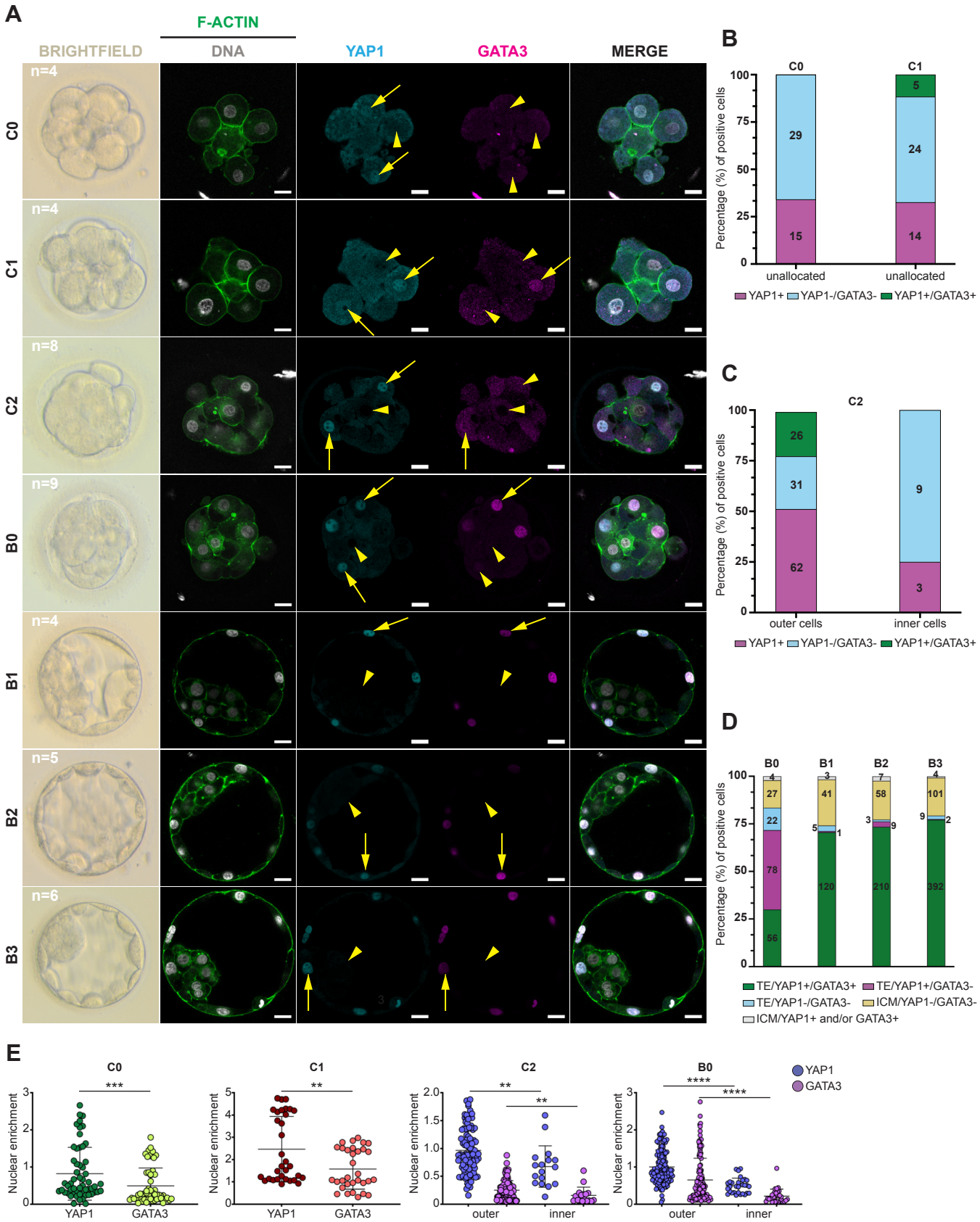
A
F-ACTIN
BRIGHTFIELD
DNA
YAP1
GATA3
MERGE
C0
C1
C2
B0
B1
B2
B3
n=4
n=4
n=8
n=9
n=4
n=5
n=6
B
C0
C1
Percentage (%) of positive cells
unallocated
unallocated
YAP1+
YAP1-/GATA3-
YAP1+/GATA3+
C
C2
outer cells
inner cells
D
B0
B1
B2
B3
TE/YAP1+/GATA3+
TE/YAP1+/GATA3-
TE/YAP1-/GATA3-
ICM/YAP1-/GATA3-
ICM/YAP1+ and/or GATA3+
E
C0
C1
C2
B0
Nuclear enrichment
YAP1
GATA3
outer
inner

Figure 4: GATA3 and YAP1 co-localize before polarity is established and mainly characterize the outer cells in human pre-implantation embryos

(A) Optical sections of embryos analysed for DNA (white), F-actin (green), YAP1 (turquoise) and GATA3 (magenta), presence indicated by yellow arrows, absence indicated by yellow arrowheads.

(B) Percentage of unallocated cells during C0 and C1 stages positive for YAP1, negative for both YAP1 and GATA3 and positive for both YAP1 and GATA3.

(C) Percentage of YAP1 and GATA3 positive/negative cells in outer and inner cells of C2 embryos.

(D) Percentage of TE and ICM cells of B0-B3 embryos positive or negative for YAP1 and/or GATA3.

(E) Nuclear enrichment of YAP1 and GATA3 in C0-B0 embryos. Mann Whitney-*U*-test, **$p<0.01$, ***$p<0.001$, ****$p<0.0001$.

Brightfield images were taken before fixation. Scale bars, 20µm.

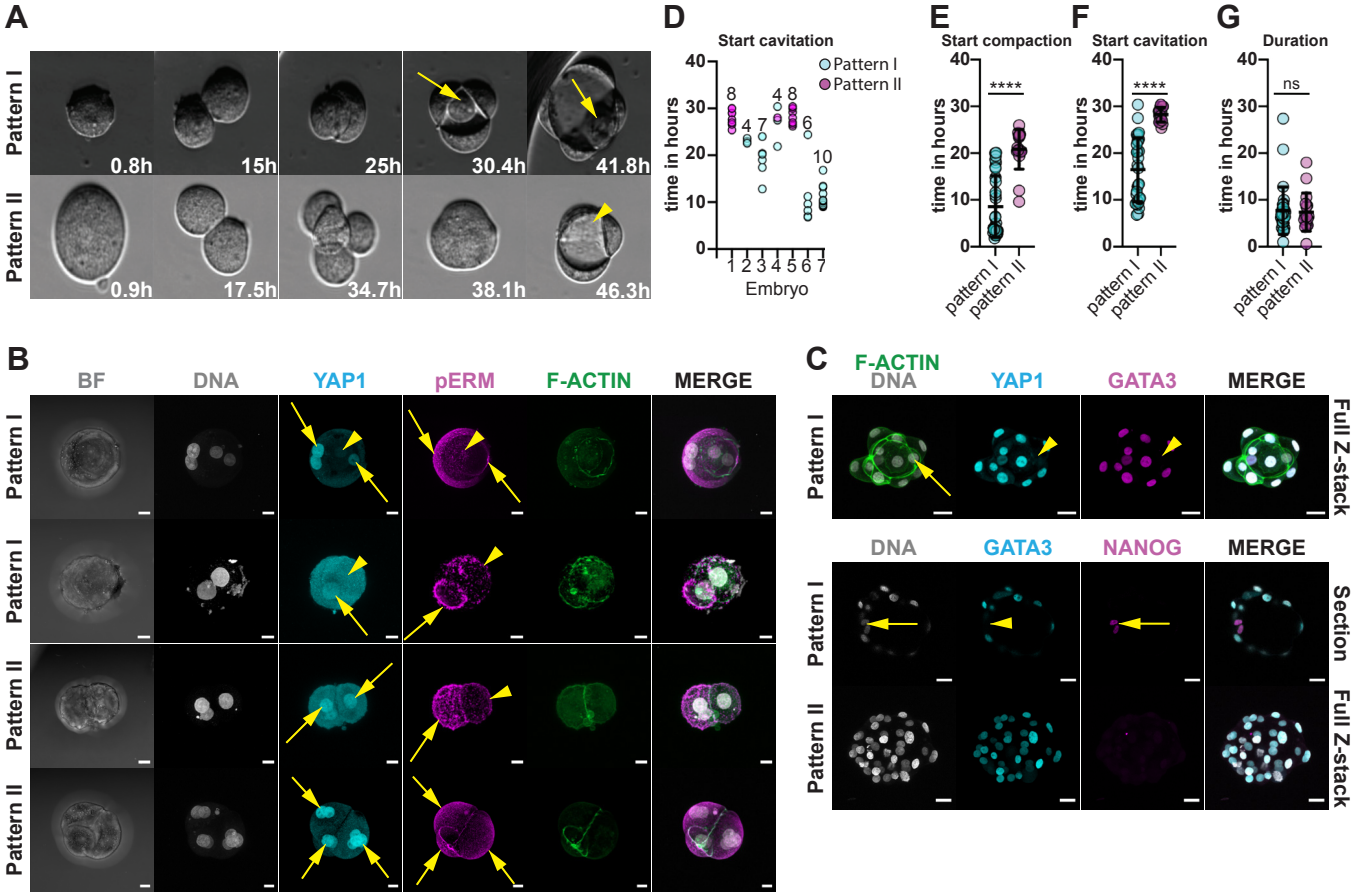
A
Pattern I
Pattern II
0.8h
15h
25h
30.4h
41.8h
0.9h
17.5h
34.7h
38.1h
46.3h
D
Start cavitation
Pattern I
Pattern II
time in hours
Embryo
E
Start compaction
****
pattern I
pattern II
F
Start cavitation
****
G
Duration
ns
B
BF
DNA
YAP1
pERM
F-ACTIN
MERGE
C
F-ACTIN
DNA
YAP1
GATA3
MERGE
Full Z-stack
NANOG
Section

Figure 5: Single human 8-cell stage blastomeres develop into mini-blastocysts following two patterns

(A) Stills at different time points (hours or h) of time-lapse videos from mini-blastocysts revealed two different patterns: in pattern I, 2/16 couplets engulfed and blastulated; in pattern II, 2/16 couplets divided into 4/32 quadruplets and blastulated without a visible ICM (yellow arrowhead).

(B) Orthogonal projections of mini-blastocysts at 4 dpf and 5 dpf analysed for DNA (white), YAP1 (turquoise), p-ERM (magenta), F-actin (green). Differences in start of compaction in hours between pattern I and pattern II.

(C) Full Z-stacks and optical sections of 6 dpf mini-blastocysts. Top panel: F-actin (green), DNA (white), YAP1 (turquoise) and GATA3 (magenta). Second and third panel: DNA (white), GATA3 (turquoise) and NANOG (magenta).

(D) Start of compaction in hours (y-axis) per embryo (1-7) (x-axis).

(E) Differences in time points of compaction in hours between pattern I and pattern II.

(F) Differences in time points of cavitation in hours between pattern I and pattern II.

(G) Differences in duration of compaction in hours between pattern I and pattern II.

Presence of signal indicated by yellow arrows, absence indicated by yellow arrowheads. Brightfield images were taken after fixation. Scale bars, 20µm. All error bars are mean ± SD.

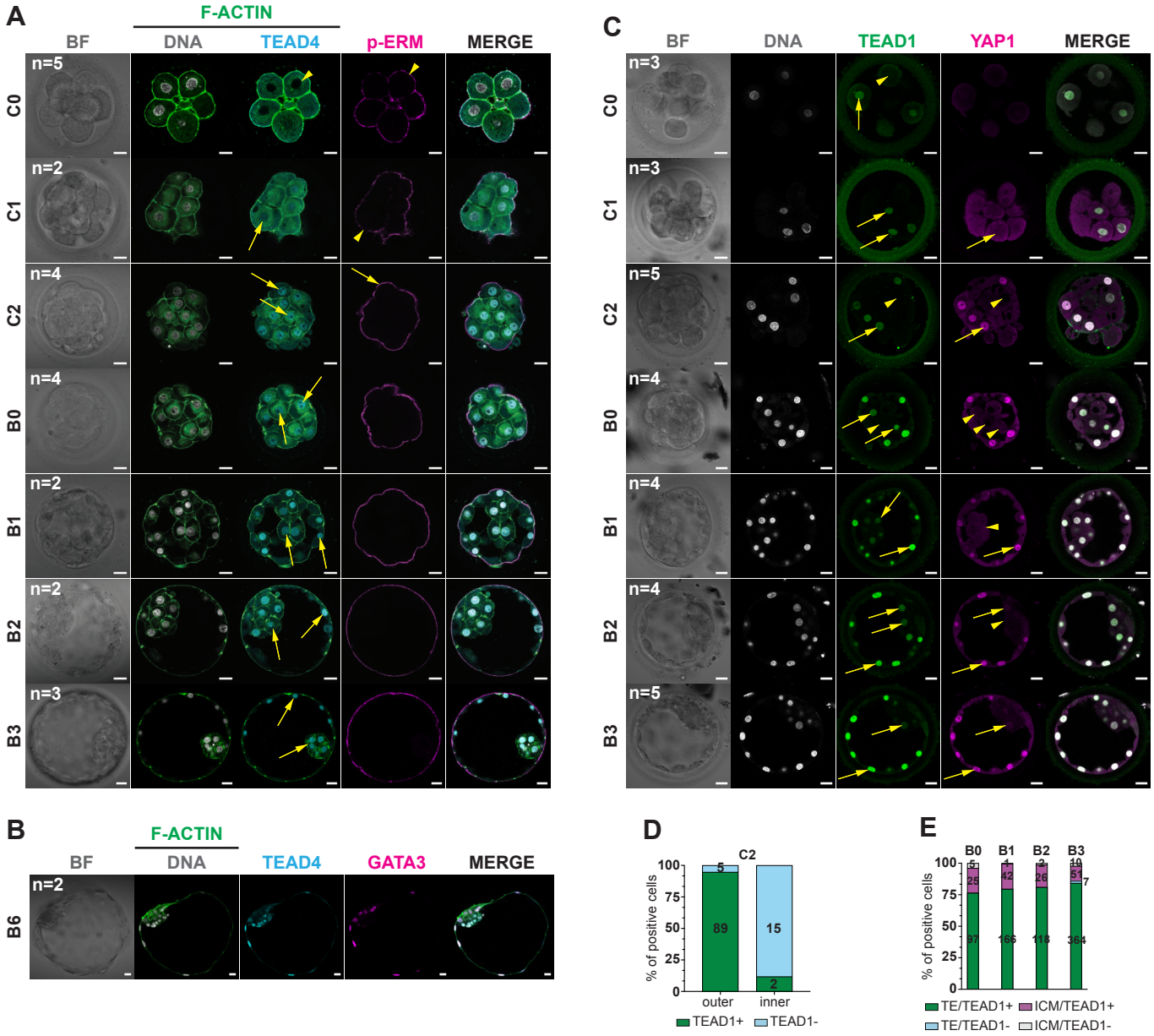
A
F-ACTIN
BF
DNA
TEAD4
p-ERM
MERGE
C0
C1
C2
B0
B1
B2
B3
n=5
n=2
n=4
n=4
n=2
n=2
n=3
C
BF
DNA
TEAD1
YAP1
MERGE
n=3
n=3
n=5
n=4
n=4
n=4
n=5
B
F-ACTIN
BF
DNA
TEAD4
GATA3
MERGE
B6
n=2
D
C2
% of positive cells
100
75
50
25
0
5
89
15
2
outer
inner
TEAD1+
TEAD1-
E
B0
B1
B2
B3
% of positive cells
100
75
50
25
0
5
25
97
1
42
166
2
26
118
10
51
364
7
TE/TEAD1+
ICM/TEAD1+
TE/TEAD1-
ICM/TEAD1-

Figure 6: TEAD4 is ubiquitously expressed in the human embryo while TEAD1 consecutively marks the trophectoderm lineage

(A) Optical sections of embryos (C0-B3) analysed for DNA (white), F-actin (green), TEAD4 (turquoise) and p-ERM (magenta).

(B) Optical section of a B6 embryo analysed for DNA (white), F-actin (green), TEAD4 (turquoise) and GATA3 (magenta).

(C) Optical sections of embryos (C0-B3) analysed for DNA (white), TEAD1 (green), YAP1 (magenta).

(D) Percentage of TEAD1 positive/negative cells at the C2 stage.

(E) Percentage of TE and ICM cells positive/negative for TEAD1 in B0-B3 stages.

Presence of signal indicated by yellow arrows, absence indicated by yellow arrowheads. Brightfield images were taken after fixation. Scale bars, 20µm.

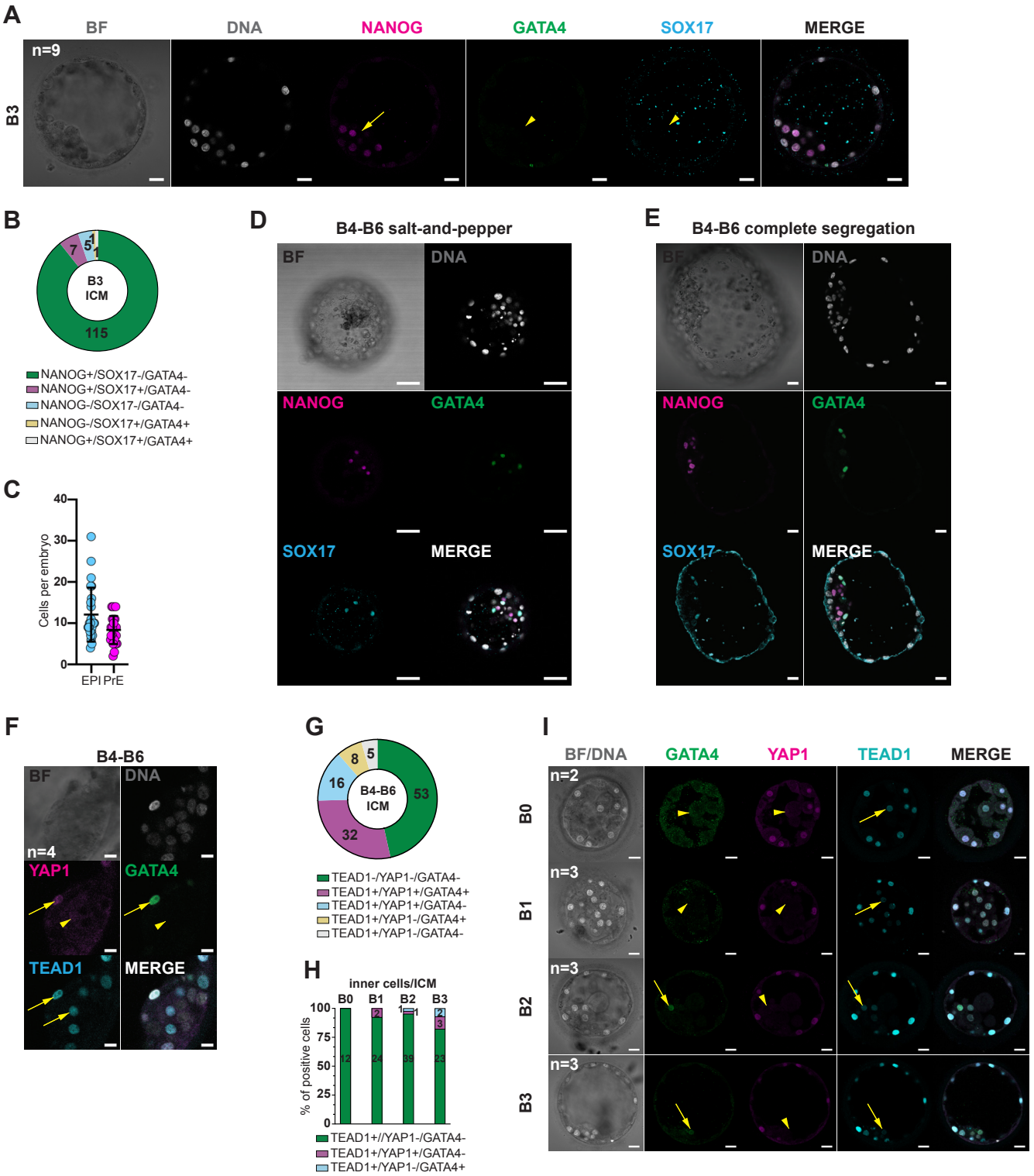
A
BF
DNA
NANOG
GATA4
SOX17
MERGE
n=9
B3
B
B3 ICM
115
7
5
1
1
NANOG+/SOX17-/GATA4-
NANOG+/SOX17+/GATA4-
NANOG-/SOX17-/GATA4-
NANOG-/SOX17+/GATA4+
NANOG+/SOX17+/GATA4+
C
Cells per embryo
40
30
20
10
0
EPI PrE
D
B4-B6 salt-and-pepper
BF
DNA
NANOG
GATA4
SOX17
MERGE
E
B4-B6 complete segregation
BF
DNA
NANOG
GATA4
SOX17
MERGE
F
B4-B6
BF
DNA
n=4
YAP1
GATA4
TEAD1
MERGE
G
B4-B6 ICM
53
32
16
8
5
TEAD1-/YAP1-/GATA4-
TEAD1+/YAP1+/GATA4+
TEAD1+/YAP1+/GATA4-
TEAD1+/YAP1-/GATA4+
TEAD1+/YAP1-/GATA4-
H
inner cells/ICM
B0
B1
B2
B3
% of positive cells
100
75
50
25
0
12
24
35
33
2
3
2
3
1
1
TEAD1+//YAP1-/GATA4-
TEAD1+/YAP1+/GATA4-
TEAD1+/YAP1-/GATA4+
I
BF/DNA
GATA4
YAP1
TEAD1
MERGE
B0
B1
B2
B3
n=2
n=3
n=3
n=3

Figure 7: YAP1/TEAD1 consecutively mark primitive endoderm

(A) Optical section of a B3 blastocyst analysed for DNA (white), NANOG (magenta), GATA4 (green), SOX17 (turquoise).

(B) Percentage of ICM cells positive/negative for NANOG, GATA4 and SOX17 at the B3 stage.

(C) Number of cells per blastocyst in the EPI and PE lineages. Counts are based on NANOG (EPI), SOX17/GATA4 (PE), TEAD1/YAP1 (TE/PE) and GATA3 (TE) protein expression.

(D) Optical section of a 6 dpf blastocyst with NANOG, GATA4 and SOX17 in salt-and-pepper constellation.

(E) Optical section of a 6 dpf blastocyst with NANOG, GATA4 and SOX17 after completed segregation.

(F) Optical section of 6 dpf blastocyst analysed for DNA (white), TEAD1 (turquoise), YAP1 (magenta).

(G) Percentage of ICM cells positive/negative for GATA4, TEAD1 and YAP1 at dpf6.

(H) Percentage of cells positive/negative for TEAD1, GATA4 and YAP1 in the ICM of B0-B3 blastocysts.

(I) Optical sections of B0-B3 blastocysts analysed for DNA (white), GATA4 (green), YAP1 (magenta) and TEAD1 (turquoise).

Presence of signal indicated by yellow arrows, absence indicated by yellow arrowheads. Brightfield images were taken after fixation. Scale bars, 20µm.